

Utilization of Spectral Information in Clustering based Color Image Segmentation

Zhengzhe Wu¹, Ville Heikkinen¹, Jussi Parkkinen^{1,2}, and Markku Hauta-Kasari¹

1) University of Eastern Finland (Finland), 2) Monash University, Sunway Campus (Malaysia)

Abstract

We studied the utilization of illumination and observer spectral characteristics in clustering based color image segmentation. Segmentation was based on *k*-means algorithm, spectral clustering algorithm and non-local spatial constraint spectral clustering algorithm both with the Nyström method. The image segmentations were performed for four different representations derived from a set of spectral images: 1) simulated sRGB images using D65 illumination, 2) six band images based on sRGB images under the D65 and A illuminations, 3) estimated spectral reflectance images, and 4) true spectral reflectance images. The spectral reflectance estimation was based on Wiener estimation model, reflectance of Macbeth Color Checker (24 samples) and CIE XYZ tristimulus values under the D65 and A illuminations. The experimental results showed that the segmentation results via reflectance estimation model were improved when compared to the segmentation with sRGB images. These results suggest that it is useful to include the knowledge from illumination and observer spectral characteristics in order to increase the clustering based color image segmentation accuracy.

Introduction

Spectral imaging has been used successfully in many research and industrial fields nowadays. These include medical imaging [1], remote sensing [2], quality control [3], and digitization of culture heritage [4]. The spectral image comprises a great number of spectral bands, usually from tens to hundreds, not only in the visible (VIS) wavelength range, but also in the ultraviolet and infrared ranges. Spectral images taken over VIS wavelength ranges provide more accurate spectral information of objects in them, compared to conventional trichromatic RGB images. This added accuracy is often a critical issue in the applications mentioned above. By utilizing spectral images, the ability to segment and recognize objects in the image is greatly enhanced [5].

Image segmentation is one of the most important tasks in image analysis and computer vision applications. In segmentation process, image can be divided into homogeneous areas based on some visually defined criteria [6]. For unsupervised spectral image segmentation, clustering methods are often used, since they need no prior knowledge from the image dataset, often obtain satisfied results, and are easy to implement. K-means (KM) algorithm is one of the simple and most popular clustering algorithms and used for image segmentation for a long time [7]. It minimizes the MSE between data points and their corresponding cluster centroids. Spectral clustering (SC) [8], a relaxation of the graph partitioning problem, has been successfully used in spectral

image segmentation [5].¹ Often Nyström method is employed with SC for image segmentation to solve the computation problem [9]. In clustering based image segmentation, spatial information of the image is usually taken into account in the clustering process [10]. As an example, non-local spectral clustering (NLSSC) includes spatial information in the original SC [11].

The segmentation based on spectral images usually return superior results to low dimensional multispectral images, such as RGB images. However, spectral imaging devices are expensive and impractical, which therefore are mainly used in laboratories. In contrast, RGB devices are inexpensive and practical. Moreover, the spectral images suffer from many other drawbacks compared with RGB images, such as large storage place, low spatial resolution, and low imaging speeds. As a result, it seems more practical to use RGB images in computer vision and object recognition tasks in most cases. However, as indicated above, RGB images cannot represent the spectral information of objects as accurate as spectral images. Due to the limitation of RGB representation, it is necessary to include some computational processing stages in the image acquisition. As an example, it may be useful to estimate reflectance spectra from RGB images in order to achieve illumination independent representation of objects in the image [12].

In this work, we studied the utilization of illumination and observer spectral characteristics in color image segmentation based on *k*-means algorithm and spectral clustering techniques (SC and NLSSC). Segmentations were performed for the true spectral reflectance images, for estimated (based on CIE XYZ tristimulus values) spectral reflectance images, and for simulated sRGB images. Firstly, based on the true spectral reflectance images, corresponding color images were simulated both in sRGB space and CIE XYZ spaces under two illuminations D65 and A respectively. Secondly, from concatenated CIE XYZ tristimulus values under D65 and A illuminations of each image, the corresponding reflectance was estimated by using Wiener estimation model based on the reflectance of Macbeth Color Checker (24 samples). Then KM, SC and NLSSC both with Nyström method were employed separately to do image segmentation on those different representations of the same image dataset, which are 1) simulated sRGB images under D65 illumination, 2) six-band sRGB image concatenated by two simulated sRGB images under D65 and A illuminant respectively, 3) estimated spectral reflectance images, and 4) true spectral reflectance images. Experiments have been done on several different images. Evaluation of segmentation results was based on manually constructed ground-truth information from simulated sRGB

¹ Please note that the word "spectral" has two different meanings in this sentence: the first one refers to eigenvalue spectrum of a matrix, and the second one is the physical energy or reflectance distribution.

images. The experimental results showed that the segmentation accuracies of simulated sRGB images under D65 were improved by using two illuminations or spectral reflectance estimation model. Therefore, it seems useful to include the knowledge from illumination and observer characteristics in the image segmentation, in order to improve the accuracy of clustering based color image segmentation.

The structure of following parts in this work is organized as follows: in section 2, image formation and Wiener reflectance estimation model will be introduced; then the spectral clustering and non-local spatial constraint spectral clustering for image segmentation will be presented; section 4 will give experimental results and the discussion; and this paper ends with conclusions.

Image Formation and Reflectance Estimation

The image formation process is affected by the light sources, object reflectance, and the spectral sensitivity of the observer. The pixel-wise response value x^i of the incoming color signal reflected from an object surface under a given illuminant can be modeled as

$$x^i = \int_{\Lambda} I(\lambda)r(\lambda)s_i(\lambda)d\lambda + \varepsilon^i \quad (1)$$

where $i=1, \dots, k$ is the number of sensor channels for this observer, Λ is the wavelength interval, I is the spectrum of the illumination, r is the reflectance of a object point, s_i is the spectral sensitivity of the observer in i^{th} channel, and ε^i is the noise that is assumed to be normally distributed in i^{th} channel [13]. The scaling factors related to the exposure setting and the measurement geometry are neglected in equation (1). In practice, the equation (1) is sampled and approximated by

$$x^i \approx \Delta\lambda \sum_{t=1}^n I(\lambda_t)r(\lambda_t)s_i(\lambda_t) + \varepsilon^i \quad (2)$$

where $\{\lambda_t\}_{t=1}^n$ is a set of uniformly sampled wavelengths and n is the number of sampled wavelengths. Let $X = (x^1, \dots, x^k)^T \in \mathfrak{R}^k$, $E = (\varepsilon^1, \dots, \varepsilon^K)^T \in \mathfrak{R}^k$, $R = (r(\lambda_1), \dots, r(\lambda_n))^T \in \mathfrak{R}^n$, $W = \Delta\lambda(w_1, \dots, w_k)^T \in \mathfrak{R}^{k \times n}$ with $w_i = (I(\lambda_1)s_i(\lambda_1), \dots, I(\lambda_n)s_i(\lambda_n))^T \in \mathfrak{R}^n$, where T represents the transpose of a matrix. Based on this notation, the response vector X can be written as,

$$X \approx WR + E \quad (3)$$

In this model, object reflectance spectrum R provides illumination independent information from object surface.

The aim of reflectance estimation is to estimate or recover object reflectance R from measurements X [13, 14]. Widely used approach is to use the Wiener estimation, defined as

$$\hat{R} = \Sigma_{RR}W^T(W\Sigma_{RR}W^T + \gamma I)^{-1}X \quad (4)$$

where Σ_{RR} is the autocorrelation of the reflectance and γ is the variance of the noise E . In our experiments, we utilized the Wiener estimation model (4) by using simulated CIE XYZ values as the measurements X . In this case, the spectral sensitivity matrix W corresponded to illumination weighted CIE color matching functions. The estimation was performed by utilizing CIE XYZ responses under D65 and A illuminations and in a noise-free manner via choice $\gamma = 0$.

Spectral Clustering for Image Segmentation

Spectral clustering (SC), a relaxation of the graph partitioning problem, is based on the eigen-decomposition of the Laplacian matrix derived from dataset [8]. Let

$X = \{x_1, \dots, x_n\}$ be a nonempty dataset where $x_i \in \mathfrak{R}^d$ and the similarity matrix or affinity matrix S with elements $s_{ij} \geq 0$ that are the similarity between each pair of data points x_i and x_j . The similarities are typically calculated by Gaussian similarity function as

$$s_{ij} = \begin{cases} \exp\left(-\frac{\|x_i - x_j\|^2}{2\sigma^2}\right) & \text{if } i \neq j \\ 0 & \text{otherwise} \end{cases} \quad (5)$$

where $\|\cdot\|$ is the Euclidean norm and σ is the scaling parameter controlling the rapidity of the decay of s_{ij} . Define degree matrix D with $d_i = \sum_{j=1}^n s_{ij}$ on its main diagonal. The normalized Laplacian matrix can be written as $L = D^{-1/2}SD^{-1/2}$. The eigenvectors obtained by the eigen-decomposition of the Laplacian matrix L , induce a new data representation of the original dataset X . By using this new representation, X can be easily clustered by any other clustering algorithms such as k-means algorithm. In addition, Nyström method is often used to estimate the eigenvectors of the Laplacian matrix L from sampled pixels, in order to solve the computational problem of SC [9]. The spectral clustering algorithm proposed in [8] combined with Nyström method for image segmentation can be written as Algorithm 1.

Algorithm 1: Spectral Clustering for Image Segmentation (SC)

Input: Input image X , the number of segments K , parameter in the Gaussian similarity function, and percentage of sampled pixels for Nyström method *perc*.

Output: Image segment labels.

Begin

1. Compute similarity matrix S and corresponding degree matrix D .
2. Utilize Nyström method to compute the eigenvectors of Laplacian matrix $D^{-1/2}SD^{-1/2}$ with *perc* percent sampled pixels.
3. Select the K eigenvectors v_1, \dots, v_K corresponding to K largest eigenvalues and store them in columns of matrix $V \in \mathfrak{R}^{n \times K}$.
4. Construct the matrix $U \in \mathfrak{R}^{n \times K}$ from V by normalizing the row vectors to have unit Euclidean length.
5. Treat each row of U as a data point, cluster U into K clusters with any clustering algorithm like k-means to obtain the segmentation result.

End

Recently, a non-local spatial spectral clustering (NLSSC) for image segmentation was proposed based on SC and showed better segmentation results than the traditional SC [11]. The idea of non-local spatial information is that if a set of pixels have a similar neighbor pixel configuration in the configuration window centered at these pixels, they are more likely to be similar [15]. Although non-local spatial information can be derived from all pixels in the image, it usually uses only the neighbor pixels in the search window due to the computational issue. The non-local spatial information \bar{x}_i for the pixel x_i can be derived from the non-local mean of all pixels in the search window defined as

$$\bar{x}_i = \sum_{j \in M_R^i} w_{ij} x_j \quad (6)$$

where M_R^i is the $R \times R$ search window centered at pixel x_i , and w_{ij} is the weight for each pixel x_j based on the similarity between all pixels in the configuration windows centered at x_i and x_j , satisfying $0 \leq w_{ij} \leq 1$ and $\sum_{j \in M_R^i} w_{ij} = 1$. Take Figure 1 for an instance, let x_i be the pixel with red background, x_j are other pixels in the black window M_R^i except for x_i . If x_j is the pixel with green background, the configuration window of x_i and x_j are red and green windows respectively. The weights w_{ij} are defined as

$$w_{ij} = \frac{1}{z_i} e^{-\frac{SI_{ij}}{H}} \quad (7)$$

where H is the filtering degree parameter controlling the decay of the weight function w_{ij} , z_i is the normalization constant that is $z_i = \sum_{j \in M_R^i} e^{-SI_{ij}/H}$, and SI_{ij} is calculated by the sum of Euclidean distance between each pixel in the $S \times S$ configuration window N_S^i and N_S^j centered at x_i and x_j respectively as $SI_{ij} = \sum_{q=1}^{S^2} \|x_q(N_S^i) - x_q(N_S^j)\|^2$ where $x_q(N_S^i)$ and $x_q(N_S^j)$ are q^{th} pixels in the configuration window N_S^i and N_S^j .

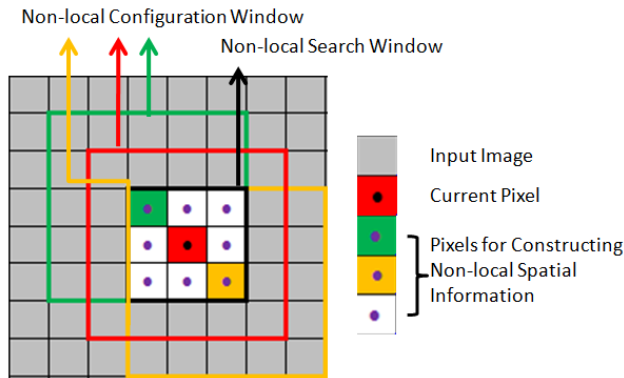


Figure 1. Illustration of non-local spatial information

In reference [11], the objective function of weighted kernel k-means algorithm (WKKM) was modified to add the non-local spatial constraint term. Based on the mathematical equivalence between SC and WKKM, the normalized Laplacian matrix $D^{-1/2}SD^{-1/2}$ in the original spectral clustering can be replaced by $W^{-1/2}AW^{-1/2}$, where

$$A_{ij} = K(x_i, x_j) + \alpha(K(x_i, \bar{x}_j) + K(\bar{x}_i, x_j)) + \alpha^2 K(\bar{x}_i, \bar{x}_j) \quad (8)$$

where $K(\cdot)$ is Gaussian similarity function with α as the scaling parameter and the diagonal matrix W is with the following element on its main diagonal

$$W_{ij} = \sum_{j=1}^n A_{ij} \quad (9)$$

As a result, the NLSSC method for image segmentation with Nyström method can be written as Algorithm 2 [11].

Algorithm 2: Non-local Spatial Constrained Spectral Clustering for Image Segmentation (NLSSC)

Input: Input image X , the number of segments K , parameter in the Gaussian similarity function, parameters of the non-local spatial constraints R, S, H , and percentage of sampled pixels for Nyström method $perc$.

Output: Image segment labels.

begin

1. Compute non-local spatial information \bar{x}_i for all pixels in input image X based on the equation (6).
 2. Compute matrix A based on equation (8).
 3. Compute diagonal weighting matrix W based on equation (9).
 4. Utilize Nyström method to compute the eigenvector of vector $W^{-1/2}AW^{-1/2}$ with $perc$ percent sampled pixels.
 5. Select the K eigenvectors v_1, \dots, v_K corresponding to K largest eigenvalues and store them in columns of matrix $V \in \mathbb{R}^{n \times K}$.
 6. Construct the matrix $U \in \mathbb{R}^{n \times K}$ from V by normalizing the row vectors to have unit Euclidean length.
 7. Treat each row of U as a data point, cluster U into K clusters with any clustering algorithm like k-means to obtain the segmentation result.
- end

Experimental Results and Discussion

This section presents the results of experiments conducted to evaluate the utilization of illumination and observer spectral characteristics for color image segmentation via k-means (KM) and spectral clustering algorithms (SC and NLSSC). By using the true spectral reflectance images, sRGB images and estimated spectral reflectance images were simulated for the experiments. All pixel vectors in these images were normalized by their Euclidean norm before segmentation in order to reduce effects due to scale differences in data [5]. Four spectral reflectance images that are available at [16] were used in experiments, which were firstly down-sampled spatially once by simply taking a pixel by every two pixels horizontally and vertically, respectively, in order to increase segmentation speed. Table 1 shows the details of those images, and their simulated sRGB representation under illuminant D65 are shown in Figure 3 (a). And all the algorithms were implemented in Matlab R2009a and tested in the desktop with Intel Core2 Duo E8400 3 GHz CPU and 3.25 GB RAM.

Table 1. The details of the spectral reflectance images used in experiments

| Image | Segments | Spatial size | Spectral Band Range |
|----------|----------|--------------|--------------------------------|
| fruits | 7 | 199 × 145 | 400 - 700 nm 10 nm interval |
| hand | 2 | 111 × 136 | 380 - 780 nm 5 nm interval |
| texture1 | 4 | 128 × 128 | 380 - 780 nm 10 nm interval |
| toy2 | 5 | 254 × 224 | 400 - 700 nm 10 nm interval |

As the final clustering results of KM are highly sensitive to the initial cluster centroids, we repeated running KM 60 times with random initialization centroids and 100 iterations each time. The final segmentation result is based on the result with the lowest MSE value between data points and their corresponding cluster centroids in the 60 runs.

Since the segmentation results of spectral clustering are quite sensitive to the selection of scaling parameter of the Gaussian similarity function, for both SC and NLSSC were tuned between [0.01, 0.02, ..., 0.09] and [0.1, 0.2, ..., 10] instead of fixing its value, in order to achieve the best segmentation accuracies of each representation of all test images. For simplicities, the parameters of the non-local spatial constraints were set to $\sigma = 0.005$, $R = 3$, $S = 5$, and $H = 600$. And 1% pixels were uniformly sampled from each image for Nyström method with $\text{perc} = 0.01$. Because KM algorithm used in the last step of SC and NLSSC is quite sensitive to the initial cluster centroids, we did the same routine as in KM based image segmentation: repeated it 60 times with random initialization and 100 iterations each time, and result with the lowest MSE value between data points and their corresponding cluster centroids in the 60 runs was chosen to be the final segmentation result.

The segmentation accuracy (SA) is defined as $SA = N_C/N_T$ based on the manually made segmentation ground truth made from simulated sRGB representation, where N_C is the number of correct segmented pixels and N_T is the number of total pixels in the image. The segment edges of ground truth for each image are shown by black lines on its corresponding sRGB image under D65 illuminant in Figure 2.

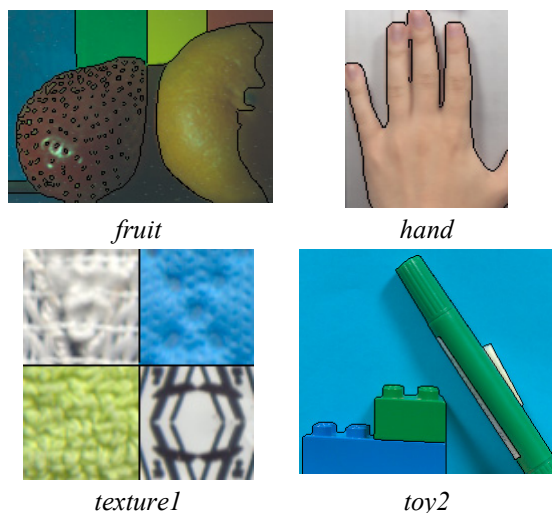


Figure 2. Illustration of the ground truth of tested images by black lines that indicate segment edges.

At first, the segmentations were done for the original true spectral reflectance images. The best segmentation accuracies of these images are quite high as shown in the columns labeled “SC” and “NLSSC” in Table 2 (“OR”). When considering the data utilized in this study, it can be assumed that original spectral reflectance images provide the most accurate representation of objects and scenes. However, the SAs of the original spectral reflectance images “hand”, “texture1”, and “toy2” based on KM are worse than those of estimated spectral reflectance images, and even worse than the SAs of sRGB images in the case of image “hand”. In order to discover the possible reasons for this, we analyzed some spectra from the original and estimated spectral reflectance images. Based on this analysis we concluded that noise in original spectral data may have significant effects for the segmentation process in some cases. Especially, it seems that this was the case for KM

algorithm. Visual evaluation indicated that some of the noise features were partly removed by the reflectance estimation process.

Secondly, color images in sRGB space under D65 and A illuminations were simulated from the spectral reflectance images. The SAs of sRGB images under D65 illumination in the columns labeled “SC” and “NLSSC” in Table 2 can be seen to be lower than those of the true spectral reflectance images, especially for the “fruit” and “texture1” images. That’s because the three channel sRGB images cannot represent spectral information as accurately as spectral reflectance images. Therefore, those results can be regarded here as the base-line for the SAs of SC and NLSSC. In addition, concatenated sRGB images with D65 and A illuminations were tested (“sRGB(D65, A)”). Here the concatenated sRGB image refers to the six-band image combined by two sRGB images with the same scene but under illuminations of D65 and A respectively. The results in Table 2 show that this six-band data lead to increased segmentation accuracies for SC and NLSSC when compared to the sRGB image under single D65 illumination. Therefore, the availability of the images of the same scene under several illuminations may improve the performance of the segmentation based on the clustering framework. This may be useful in practice, since it is relatively easy in some cases to utilize several illuminations. However, the performance of six-band data with KM lead to worse results for “hand” and “toy2” images when compared to the sRGB image under D65 illumination. This suggests that in these cases the six-band data emphasizes noises rather than informative spectral features.

Finally, we present the segmentation results for estimated spectral reflectance data in Table 2 (“ER”). The estimated data is based on the Wiener inversion model in a noise-free manner and six-band simulated XYZ tristimulus values (without normalization factor) under D65 and A illuminants. Autocorrelation matrix of Wiener operator was constructed by using reflectance data of Macbeth ColorChecker (24 samples). The SAs suggest that in most cases the results are improved when compared to those of the corresponding sRGB data. We can see that the SAs of the “toy2” image in SC and NLSSC cases are quite close to those of the true spectral reflectance images and there is a large improvement of the SAs for the “fruit” image. Moreover, it seems that the estimated reflectance images worked quite well also in the case of simple KM algorithm. It is interesting to see that the performances of KM for estimated reflectance images overcome those for the true reflectance image in some images. Although it seems that the simple KM could not handle the noises when segmenting the true spectral reflectance images compared to more advanced SC and NLSSC, the reflectance estimation model somehow partly removed the noises and improved the segmentation results in KM. It should be noted that the training reflectance data used in Wiener estimation probably contains only weak reflectance information (Macbeth Color Checker) with respect to reflectance images used in this study. It can be expected that segmentation results of estimated reflectance images can be further improved if some larger sets of more representative (with respect to images to be segmented) training data are available and such reflectance estimation model is chosen ([14]) that is able to utilize this added information more efficiently.

Table 2. Best segmentation accuracies of different representations of color images based on k-means, SC, and NLSSC. Those representations include OR – original true spectral reflectance images, sRGB(D65) – simulated sRGB images under illuminant D65, sRGB(D65, A) – concatenated simulated sRGB images under illuminants D65 and A, and ER – estimated spectral reflectance images.

| Image | | k-means | SC | NLSSC |
|----------|--------------|---------|-------|-------|
| fruit | OR | 81.75 | 87.53 | 87.10 |
| | sRGB(D65) | 74.93 | 80.29 | 80.52 |
| | sRGB(D65, A) | 76.32 | 82.07 | 83.23 |
| | ER | 80.70 | 84.04 | 84.05 |
| hand | OR | 96.96 | 98.15 | 97.90 |
| | sRGB(D65) | 97.72 | 97.89 | 97.91 |
| | sRGB(D65, A) | 97.21 | 97.90 | 97.91 |
| | ER | 97.08 | 97.86 | 97.86 |
| texture1 | OR | 80.72 | 93.50 | 93.65 |
| | sRGB(D65) | 57.82 | 83.35 | 83.35 |
| | sRGB(D65, A) | 57.89 | 83.14 | 83.12 |
| | ER | 83.08 | 84.36 | 84.24 |
| toy2 | OR | 98.40 | 98.58 | 98.69 |
| | sRGB(D65) | 98.36 | 98.14 | 97.90 |
| | sRGB(D65, A) | 96.71 | 98.20 | 98.17 |
| | ER | 98.46 | 98.52 | 98.64 |

The best segmentation results of the estimated spectral reflectance images by SC and NLSSC are visually shown by black lines showing the segment edges on corresponding sRGB images under D65 illuminant in the Figure 3 (b) and (c). Visually, it can be seen that the estimated reflectance data performs well in the segmentation tasks. The results for the “hand” and “toy2” images are satisfied and shaded parts are also segmented correctly. The “fruit” and “texture1” images are relative difficult to segment, since the former one has many shadows and similar colors and the latter one contains texture structure. Therefore, their segmentation results are relative poor compared to those of the previous two images.

The computational time of KM, SC, and NLSSC for different representation of image “fruit” is given in Table 3. For KM, it is the average computational time of 60 runs. And for SC and NLSSC, it is the average computational time of all tuned values. Also the computational time of KM in the last step of SC and NLSSC is calculated in average of 60 runs. It can be seen that the KM is much faster compared to SC and NLSSC. And NLSSC is the slowest one among these three approaches for segmenting image “fruit”.

Based on the SAs of SC and NLSSC in Table 2, it seems that it is not beneficial to choose NLSSC over the simpler SC. The performances of these algorithms were almost the same for every image. However, since the spatial parameters of the NLSSC were fixed here, more work is needed to evaluate segmentation performances between these models.

Table 3. The average computational time (s) of image “fruit”

| Representation | k-means | SC | NLSSC |
|----------------|---------|-------|-------|
| OR | 1.87 | 14.08 | 53.68 |
| sRGB(D65) | 0.22 | 12.56 | 44.28 |
| sRGB(D65, A) | 0.30 | 13.03 | 44.96 |
| ER | 1.95 | 14.51 | 54.17 |

Conclusion

In this work, the utilization of illumination and observation spectral characteristics in color image segmentation was studied. In the experiments, four different representation of the image dataset, 1) simulated sRGB images under D65 illuminant, 2) six band simulated sRGB images under D65 and A illuminants, 3) estimated spectral reflectance images, and 4) true spectral reflectance images, were segmented separately by k-means algorithm, spectral clustering and non-local spatial constraint spectral clustering. The experimental results showed that the segmentation accuracies of sRGB images (originating from single illumination) were improved by using two illuminations and/or spectral reflectance estimation model. As a result, it seems to be useful to include the knowledge of illumination and observer spectral characteristics in the color image segmentation in order to improve the accuracy of the clustering based image segmentation.

Acknowledgement

The first author thanks the support of the Academy of Finland grant 123193.

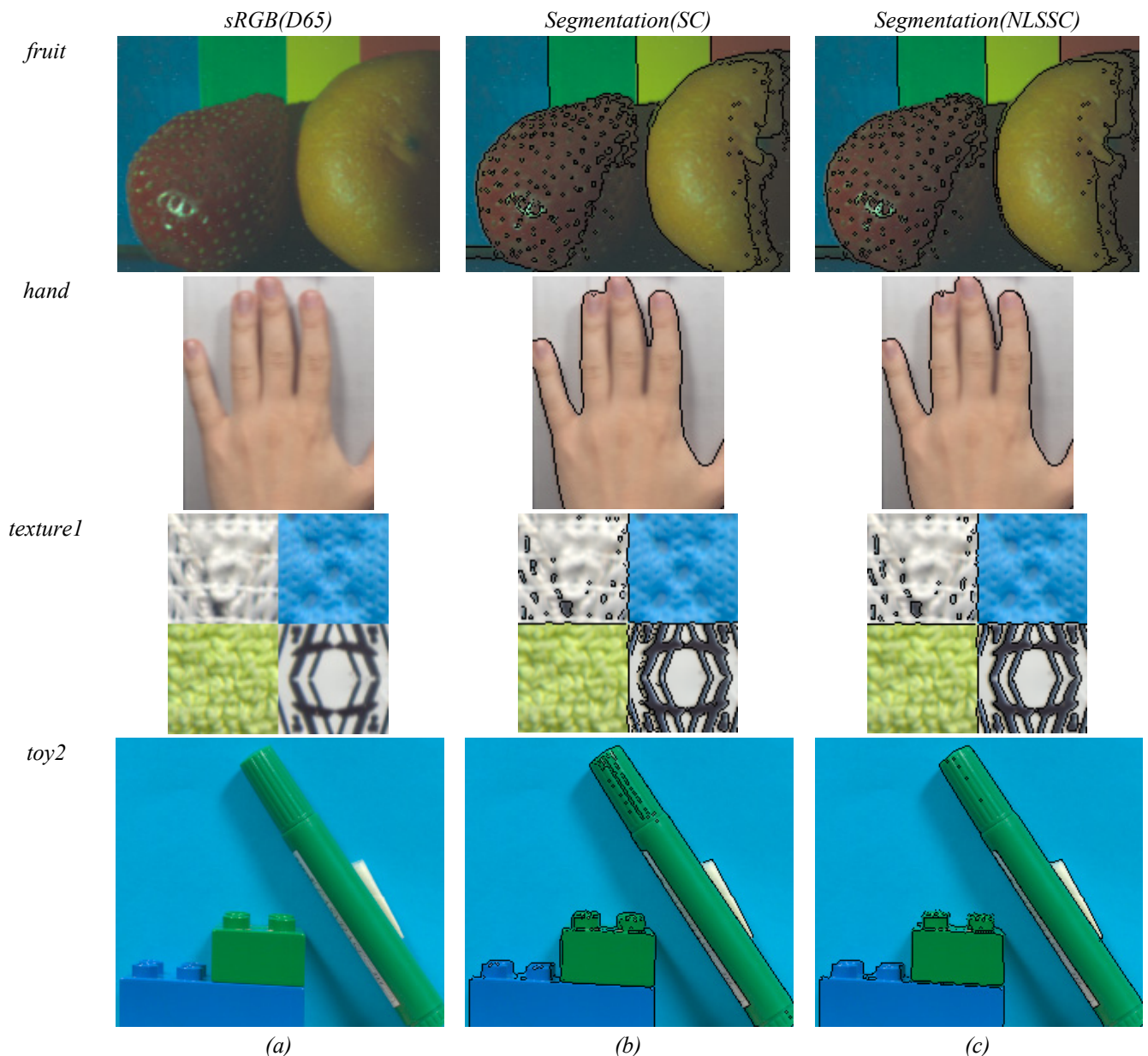


Figure 3. (a) Simulated sRGB representation of the spectral images under D65 illuminants used in the experiments; (b) and (c) best segmentation results of SC and NLSSC respectively based on the estimated spectral reflectance images visually shown by black lines that indicate segment edges.

References

- [1] P. Fält, J. Hiltunen, M. Hauta-Kasari, I. Sorri, V. Kalesnykiene, J. Pietilä, and H. Uusitalo, Spectral imaging of the human retina and computationally determined optimal illuminants for diabetic retinopathy lesion detection, *Journal of Imaging Science and Technology*, vol. 55, iss.3, pp. 030509-(10), 2011.
- [2] V. Heikkinen, T. Tokola, J. Parkkinen, I. Korpela and T. Jääskeläinen, Simulated Multispectral Imagery for Tree Species Classification Using Support Vector Machines, *Geoscience and Remote Sensing, IEEE Transactions on*, vol.48, no.3, pp.1355-1364, March 2010.
- [3] S. Kukkonen, H. Kälviäinen, J. Parkkinen, Color features for quality control in ceramic tile industry, *Optical Engineering*, vol. 40, iss. 2, pp. 170-177, 2001.
- [4] K. Miyata, H. Laamanen, T. Jääskeläinen, M. Hauta-Kasari, and J. Parkkinen, Application of spectral information to investigate historical materials -detection of metameric color area in icon images-, in *Proceedings of SCIA 2005*, Joensuu, Finland, June 19 - 22, 2005, *Lecture Notes in Computer Science* 3540, pp. 369-378, 2005.
- [5] H. Li, V. Botchko, T. Jääskeläinen, J. Parkkinen, and I. Shen, Kernel-based spectral color image segmentation, *Journal of Optical Society of America A*, vol. 25, iss. 11, pp. 805-2816, 2008.
- [6] M. Sonka, V. Hlavac, and R. Boyle, *Image processing, analysis and machine vision*, Second Edition. International Thomson, 1999.
- [7] K.S. Fu, J.K. Mui, A survey on image segmentation, *Pattern Recognition*, vol. 13, iss. 1, pp. 3-16, 1981.
- [8] A. Ng, M. Jordan, and Y. Weiss, On spectral clustering: Analysis and an algorithm, in *Advances in Neural Information Processing Systems* 14, 2001.
- [9] C. Fowlkes, S. Belongie, F. Chung, J. Malik, Spectral grouping using the Nystrom method, *Pattern Analysis and Machine*

- Intelligence, IEEE Transactions on , vol.26, no.2, pp.214-225, Feb. 2004.
- [10] S.C. Chen and D.Q. Zhang, Robust image segmentation using FCM with spatial constraints based on new kernel-induced distance measure, IEEE Trans. Syst. Man Cybern. B, vol. 34, pp. 1907-1916, 2004.
- [11] H.Q. Liu, L.C. Jiao, and F. Zhao, Non-local spatial spectral clustering for image segmentation, Nerocomputing, vol. 74, pp. 461-471, 2010.
- [12] V. Heikkinen, T. Jetsu, J. Parkkinen, M. Hauta-Kasari, T. Jaaskelainen, and S. Lee, Regularized learning framework in the estimation of reflectance spectra from camera responses, J. Opt. Soc. Am. A 24, 2673-2683, 2007.
- [13] N. Shimano, "Recovery of spectral reflectances of objects being imaged without prior knowledge," Image Processing, IEEE Transactions on , vol.15, no.7, pp.1848-1856, July 2006.
- [14] V. Heikkinen, R. Lenz, T. Jetsu, J. Parkkinen, M. Hauta-Kasari, and T. Jääskeläinen, Evaluation and unification of some methods for estimating reflectance spectra from RGB images, J. Opt. Soc. Am. A 25, 2444-2458, 2008.
- [15] A. Buades, B. Coll, and J. M. Morel, A non-local algorithm for image denoising, in Proceedings of IEEE Int. Conf. Comput. Vision Pattern Recognition, pp. 60-65, 2005.
- [16] Spectral Image Database, University of Eastern Finland Color Group, <http://spectral.joensuu.fi/>.

Author Biography

Zhengzhe Wu received his M.Sc. degree in computer science from the University of Eastern Finland, Finland, and another M.Sc. degree in optics, image, and vision from the University Jean Monnet, France, both in 2011. He is currently pursuing the Ph.D. degree in computer science in color research group at School of Computing, University of Eastern Finland.

Ville Heikkinen received the M.Sc. degree in applied mathematics from the University of Joensuu, Joensuu, Finland in 2004 and the Ph.D. degree in computer science from the University of Eastern Finland, Joensuu, Finland in 2011. He is currently post-doctoral researcher with the School of Computing, University of Eastern Finland.

Jussi Parkkinen received his M.Sc. in medical physics in 1982 and his Ph.D. in mathematics in 1989, from the University of Kuopio, Finland. He is a professor of Computer Science at the University of Eastern Finland, Finland. Since September 2011 he is on three years leave-of-absence for being professor and Head of Discipline of Electrical and Computer Systems Engineering at the Monash University Sunway Campus in Kuala Lumpur, Malaysia.

Markku Hauta-Kasari received his MSc in computer science from the University of Kuopio, Finland, in 1994 and his PhD in information processing from the Lappeenranta University of Technology, Finland, in 1999. Currently, he is Research Director and Professor in SIB-labs at the University of Eastern Finland, Finland.